Received: 23 September 2016 | Accepted: 24 October 2016 | Published on: 29 March 2017

DOI: 10.1002/asna.201713349

ORIGINAL ARTICLE

Astronomische Nachrichten

X-ray selection of Compton-Thick AGN at high redshift

G. Lanzuisi[1,2*]

[1]Dipartimento di Fisica e Astronomia, Universitá degli studi di Bologna, Bologna, Italy
[2]INAF – Osservatorio Astronomico di Bologna, Bologna, Italy

***Correspondence**
G. Lanzuisi, Dipartimento di Fisica e Astronomia, Universitá degli studi di Bologna, Via Ranzani 1, 40127 Bologna, Italy.
Email: giorgio.lanzuisi2@unibo.it

Compton-Thick (CT) active galactic nuclei (AGN) are a key ingredient of cosmic X-ray background (CXB) synthesis models, but are still an elusive component of the AGN population beyond the local universe. Multiwavelength surveys are the only way to find them at $z > \sim 0.1$, and a deep X-ray coverage is crucial in order to clearly identify them among star-forming galaxies. As an example, the deep and wide COSMOS survey allowed us to select a total of 34 CT sources. This number is computed from the 64 nominal CT candidates, each counted for its $N_{\rm H}$ probability distribution function. For each of these sources, rich multiwavelength information is available, which is used to confirm their obscured nature by comparing the expected AGN luminosity from spectral energy distribution fitting with the absorption-corrected X-ray luminosity. While *Chandra* is more efficient, for a given exposure, in detecting CT candidates in current surveys (by a factor ~ 2), deep *XMM–Newton* pointings of bright sources are vital to fully characterize their properties, for example, $N_{\rm H}$ distribution above 10^{25} cm^{-2}, reflection intensity, etc., all crucial parameters of CXB models. Since luminous CT AGN at high redshift are extremely rare, the future of CT studies at high redshift will have to rely on the large-area surveys currently under way, such as XMM-XXL and Stripe82, and will then require dedicated follow-up with *XMM–Newton*, while waiting for the advent of the ESA mission *Athena*.

KEYWORDS

galaxies, active – X-rays, galaxies

1 | INTRODUCTION

We know, since the late 1990s, that a large fraction (up to 30%) of local active galactic nuclei (AGN) are obscured by large amounts of gas and dust (e.g., Risaliti et al. 1999), above the Compton-thick[1] threshold (CT, $N_{\rm H} \geq \sigma_T^{-1} \sim 1.5 \times 10^{24}$ cm^{-2}). A similar fraction of CT AGN is required in most cosmic X-ray background (CXB) synthesis models (e.g., Comastri et al. 1995; Gilli et al. 2007): their flat spectrum is needed to reproduce the hump at 20–30 keV observed in the CXB (e.g., Ballantyne et al. 2011). However, the value of the CT fraction that one can derive is largely uncertain (Treister et al. 2009; Ueda et al. 2014) due to degeneracies between several model parameters, that is, primary continuum photon index, reflection fraction, $N_{\rm H}$ distribution above 10^{24} cm^{-2}, and high energy cut-off (see, e.g., Akylas et al. 2012).

A population of even more deeply obscured sources ($N_{\rm H} \geq 10^{25}$ cm^{-2}) may be required (Comastri et al. 2015) to reconcile new estimates of the black hole (BH) mass function in the local universe (Kormendy & Ho 2013) with that inferred by integrating the luminosity function of observed AGN via the continuity equation (e.g., Marconi et al. 2004; Soltan 1982). These heavily obscured sources, however, will not contribute much to the CXB, since even the highest energy X-rays they produce are blocked by the obscuring material.

Despite their expected large number, CT AGN are very difficult to identify beyond the local universe, resulting in a small/negligible fraction of CT AGN blindly identified in deep X-ray surveys (e.g., Lanzuisi et al. 2013; Marchesi et al. 2016a; Tozzi et al. 2006). Even NuSTAR, which is sensitive above 10 keV, was able to put only upper limits to the fraction of CT AGN at $z = 0.5 - 1$ (Alexander et al. 2013). Therefore,

[1]At these high column densities, the obscuration is mainly due to Compton scattering rather than photoelectric absorption.

several multiwavelength techniques have been developed in the past decade, based on known CT AGN broad-band properties, to preselect CT AGN beyond the local universe. IR spectral features, IR colors, or mid-IR versus optical or X-ray flux ratios can be used to select red, dusty sources at $z \sim 2$ (e.g., Houck et al. 2005; Lacy et al. 2004; Martinez-Sansigre et al. 2005). High-ionization optical emission lines from the narrow-line region, such as [OIII] and [NeV] can be used to select sources with a deficit in the observed X-ray emission, which can be ascribed to strong obscuration of the nucleus (e.g., Gilli et al. 2010; Mignoli et al. 2013; Vignali et al. 2006).

In all these cases, however, the X-ray information (either detections or staking) is crucial to unambiguously identify a fraction of CT AGN among inactive galaxies with similar properties (e.g., Fiore et al. 2008; Georgantopoulos et al. 2011; Lanzuisi et al. 2009; Vignali et al. 2014). X-rays are indeed able to provide the smoking gun of the CT nature of these sources, thanks to the unique spectral signatures observable, that is, the flat continuum and the strong Fe K emission line at 6.4 keV. Furthermore, above $L_X \sim 10^{42}$ erg s^{-1}, the contamination by star-forming galaxies in the 2–10 keV is limited. Finally, X-ray spectroscopy is favored by the redshift effect: going at high redshift, the Compton hump at 20–30 keV becomes observable by Chandra and XMM–Newton and the Fe kα line moves toward lower energies, where the effective area of current telescopes is larger.

There are, however, important caveats to take into account: (a) The fraction of CT AGN steeply rises from ~ 0 to the intrinsic value (e.g., 0.3–0.4) only below a certain flux (e.g., $F << 10^{-15}$ erg cm^{-2} s^{-1} in the 2–10 keV band) and therefore it is mandatory to reach deep sensitivities, in order to collect sizable samples of CT AGN; (b) CT AGN are a factor 30–50 fainter than normal AGN below 10-keV rest frame, requiring long exposures to collect even few tens of X-ray counts per source; (c) The transition between Compton-thin and Compton-thick is smooth, and the spectra of sources just above/below the CT threshold are very similar (Murphy & Yagoob 2009), requiring a tailored analysis (see e.g., Buchner et al. 2015) and possibly the use of the full N_H probability distribution function (PDF) when counting/selecting CT AGN, in order to avoid misclassification in one direction or the other.

For all these reasons, even in the deepest X-ray fields, different analyses of the same datasets (e.g., Brightman & Ueda 2012; Georgantopoulos et al. 2013; Tozzi et al. 2006) give different results, which are not always in agreement (see Castello-Mor et al. 2013).

Here we present results from the analysis of the large COSMOS-Legacy catalog, which allowed us to select 64 CT AGN candidates among the $\sim$4,000 point-like sources. For each candidate, the full PDF of the N_H is taken into account, to weight each source by its probability of being CT. The log N–log S curve of CT AGN in three redshift bins (up to $z = 3.5$) is also presented.

2 | SAMPLE SELECTION

2.1 | The COSMOS survey

The 2 deg^2 area of the HST COSMOS Treasury program is centered at 10:00:28.6, +02:12:21.0 (Scoville et al. 2007). The field has a unique deep and wide multiwavelength coverage, from the optical band (Hubble, Subaru, VLT, and other ground-based telescopes), to the infrared (Spitzer, Herschel), X–ray (XMM–Newton, Chandra, and NuSTAR) and radio bands. Large, dedicated ground-based spectroscopy programs in the optical region with all the major optical telescopes have been completed. Very accurate photometric redshifts are available for both the galaxy (Ilbert et al. 2009) and AGN (Salvato et al. 2011) populations.

The COSMOS field has been observed with XMM–Newton for a total of $\sim$1.5 Ms at a rather homogeneous depth of $\sim$60 ks over $\sim$2 deg^2 (Cappelluti et al. 2009; Hasinger et al. 2007), and by Chandra with a deeper observations of $\sim$160 ks: the central deg^2 was observed in 2006–2007 (Civano et al. 2012; Elvis et al. 2009) for a total of 1.8 Ms, while an additional 1.2 deg^2 was covered recently (2013–2014) by the Chandra COSMOS-Legacy survey, for a total of 2.8 Ms (Civano et al. 2016; Marchesi et al. 2016a).

The Chandra catalog used in this work includes 4016 point-like sources (from a total of 4.6 Ms of Chandra observation) detected in at least one of the following three bands: full (F; 0.5–7 keV), soft (S; 0.5–2 keV), and hard (H; 2–7 keV). Each source was detected in at least one band with probability of being a spurious detection $P < 2 \times 10^{-5}$.

2.2 | X-ray spectral analysis

One-thousand nine-hundred and forty-nine sources in the COSMOS-Legacy catalog have more than 30 counts (with average $\sim$ 145 and median $\sim$ 68 counts). This threshold allows us to derive the basic spectral properties (N_H, L_X, see Lanzuisi et al. 2013). The result of a systematic spectral analysis of all these sources is presented in Marchesi et al. (2016b). The procedure described there, however, is not optimized to look for CT AGN, since at such high column densities the simple power-law plus photoelectric absorption model does not reproduce any more the physical processes involved.

We reanalyzed all the available spectra using the BNTorus model (Brightman & Nandra 2011), specifically developed to model the obscuration at CT regimes. The geometry of the obscuring material is a spherical torus, which is essentially a sphere with a biconical aperture. We used the model with a fixed photon index $\Gamma = 1.9$ and with a fixed torus half-opening angle (60°) and inclination angle (80°). The model is therefore very simple, as it uses a single geometry and does not allow any variation between the primary continuum and the reflection/line component, or for different values of N_H between the absorber and the reflector[2]. However,

[2]As, for example, MYTorus in the decoupled version is able to do (Murphy & Yagoob 2009).

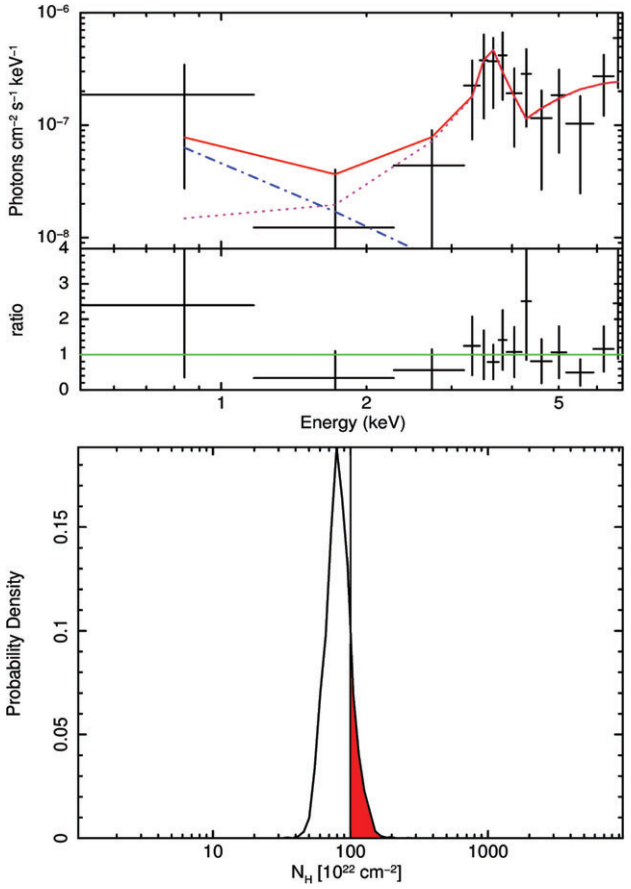

FIGURE 1 (a) Unfolded spectrum and data/model ratio of the CT candidate LID_633 at $z = 0.706$. In magenta is shown the BNtorus component, in blue the soft power law, and in red the total. (b) PDF of $N_{\rm H}$ for the spectrum shown above.

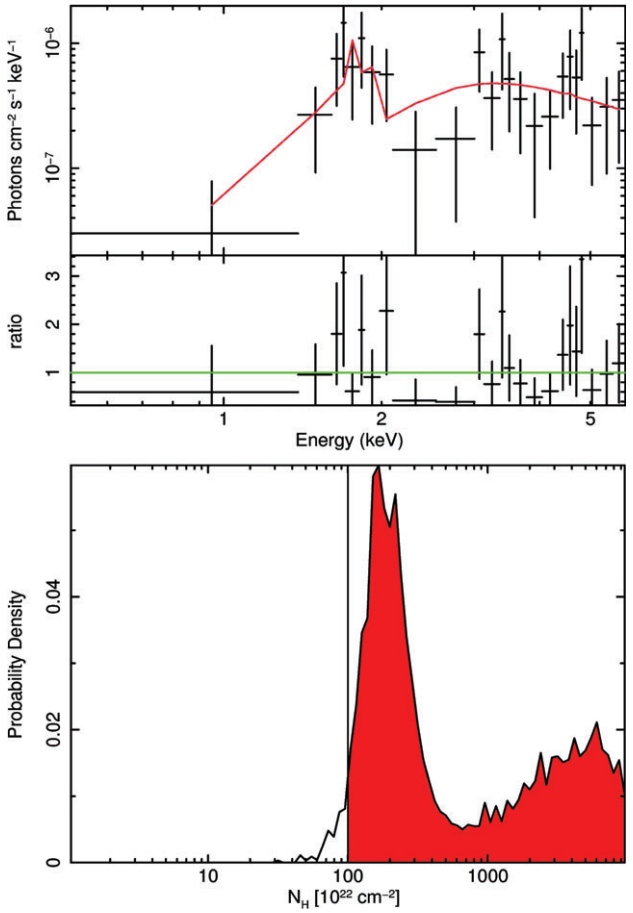

FIGURE 2 (a) Unfolded spectrum and data/model ratio of the CT candidate LID_1002 at $z = 2.612$. This source required only the BNtorus component. (b) PDF of $N_{\rm H}$ for the same source.

this choice is forced by the very limited number of counts available for each source (65% of the final CT sample has less than 50 net counts). In addition to the BNTorus model, we used a secondary power law, with the photon index fixed to 1.9, to model the emission emerging in the soft band in most of the obscured spectra (Lanzuisi et al. 2015a). The normalization of this component is forced to be $< 10\,\%$ of the primary component.

Once the best fit is obtained, we run a Monte Carlo Markov chain (MCMC) within Xspec (v. 12.8.2), to evaluate the $N_{\rm H}$ PDF. In this way, we can collect a sample of CT AGN candidates by counting each source that is close to the CT boundary, only for the part of the PDF that exceeds this boundary. Figures 1 and 2 show the unfolded spectra and residuals for two CT AGN selected in this way. The bottom panels show the $N_{\rm H}$ PDF (in red the part of the PDF that is taken into account to weight the source). Thanks to this analysis, we were able to select a sample of 64 obscured sources at $0.04 < z < 3.46$, having $> 5\,\%$ probability of being CT (i.e., a fraction of them is not nominally CT). By summing up only the fraction of the PDF of each source that is above 10^{24} cm^{-2}, we obtained a number of CT sources as $N_{CT} = 33.85$.

3 | RESULTS

The sample of the selected CT candidates spans a wide range in redshift, $0.04 < z < 3.46$ (50% of them have a photometric redshift) and absorption-corrected X-ray luminosity, $43.5 < \mathrm{Log}(\,L_{\rm X}\,) < 45.8$ erg s^{-1}, with the exception of source LID_1791 having $\log(L_{\rm X}) = 42.2$ erg s^{-1} at $z = 0.04$, identified as a CT AGN in Civano et al. (2015)[3].

Given the large correction applied due to the obscuration, almost all the sources in the sample are in the quasar regime ($L_{\rm X} > 10^{44}$ erg s^{-1}, see blue points in Figure 3). In order to verify whether these luminosities are reasonable, and therefore whether our estimate of the obscuration is correct and not overestimated, we verified that the X-ray luminosity derived after correcting for the obscuration is consistent, within ~ 1 dex, with the mid-IR AGN luminosity as computed from the spectral energy distribution (SED) fitting (either from Delvecchio et al. 2015 or Suh et al. 2016), after removing the host star-formation emission. Figure 3 shows the distribution of the AGN mid-IR (6 μm) luminosity versus the absorption-corrected $L_{\rm X}$ for the $\sim 2{,}000$ sources analyzed in

[3]This source is one of the two, with LID_633, that is detected with NuSTAR. The $N_{\rm H}$ values are consistent between our fit and those performed using also the hard X-ray data (Zappacosta et al. 2017 in prep.).

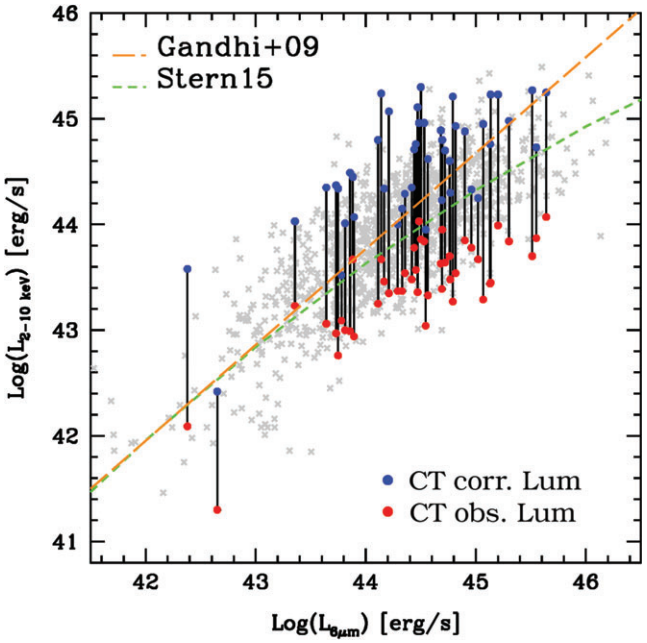

FIGURE 3 Distribution of the AGN mid-IR (6 μm) luminosity, as derived from SED fitting, after subtracting the host star-formation emission, and the 2–10 keV luminosity, for the ∼2,000 sources analyzed in Marchesi et al. (2016a) (gray crosses). Red circles show the observed L_X for the CT candidates, while blue circles show the absorption-corrected L_X. The orange (green) curve shows the relation published in Gandhi et al. (2009) (Stern 2015).

Marchesi et al. 2016b (gray crosses). Red circles show the observed L_X of the CT candidates, while blue circles show the absorption-corrected L_X.

Almost all our CT AGN have their $L_{6\,\mu m} - L_X$ within the typical scatter from the average relation (the orange or green curves, the $L_{6\,\mu m} - L_X$ relations published in Gandhi et al. 2009 and Stern 2015, respectively). However, the vast majority lie in the upper part of the distribution: this is a clear selection effect (see, e.g., Lanzuisi et al. 2015a) due to the fact that CT sources with intrinsic L_X in the lower part of the diagram would not have been detected in X-rays, having an absorbed L_X (and hence flux) below the detection threshold of the survey. This already tells us that, despite our effort, a sizable fraction of CT AGN is still missing because of their low X-ray fluxes.

3.1 | Log *N*–log *S*

To overcome this incompleteness, we can look at the log *N*–log *S* distribution, where we can compare CXB models with the number of sources detected above the flux threshold of the survey. To investigate a possible variation of the CT fraction with redshift, we divided the sample into three redshift bins and compared the observed log *N*–log *S* with the one predicted by the Akylas et al. (2012) model (Figure 4).

This model assumes $\Gamma = 1.9$, a high-energy cut-off of 195 keV, and a fraction of the reflected component flux with respect to the primary power law of 0.05 in the 2–10 keV band. To match the observed log *N*–log *S* of the CT AGN

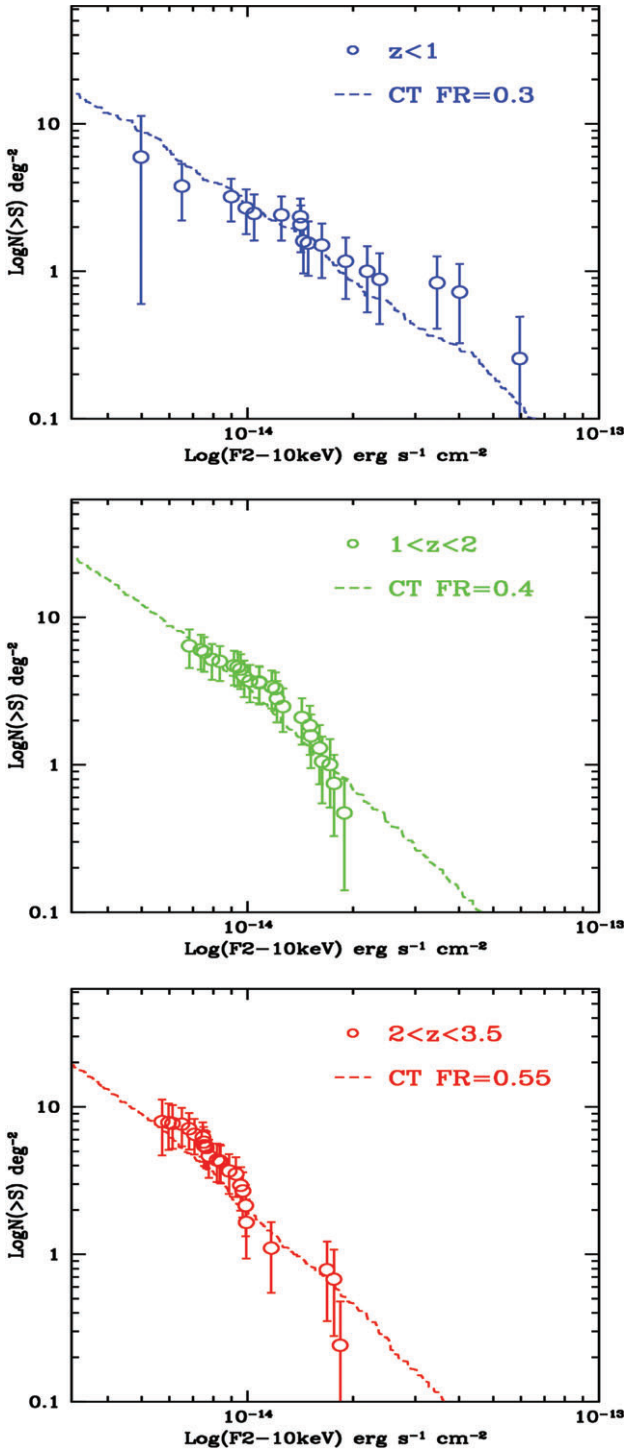

FIGURE 4 Observed log *N*–log *S* of CT candidates at $z < 1$ (top), $1 < z < 2$ (center), and $2 < z < 3.5$ (bottom), compared with the model of Akylas et al. (2012), with different CT fractions (FR).

selected in COSMOS, the fraction of sources in the $\log(N_H)$ bins 24–26 (equally distributed between the 24–25 and 25–26 bin) must increase from 30% in the $z < 1$ bin, to 40% in the $1 < z < 2$, up to 55% in the $2 < z < 3.5$ bin. These fractions are systematically higher than that predicted from other CXB models such as those of Gilli et al. (2007) and Treister et al. (2009).

Brightman and Ueda (2012) have already found a hint of an increase of the CT fraction from $z < 0.1$ (20% derived in Bur-

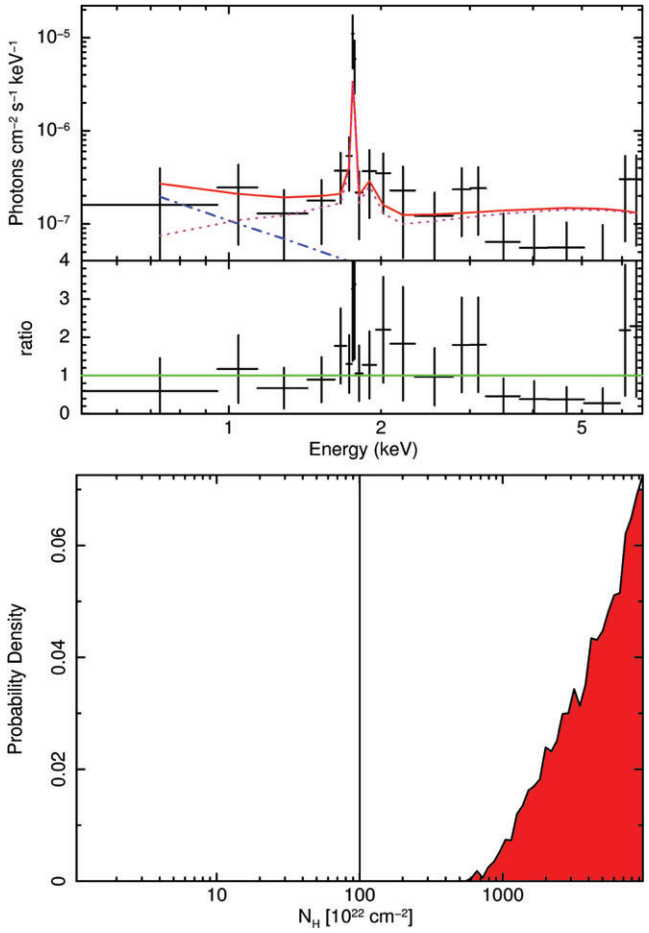

FIGURE 5 (a) Unfolded spectrum and data/model ratio of the heavily CT candidate CID_708. (b) PDF of N_H for the same source.

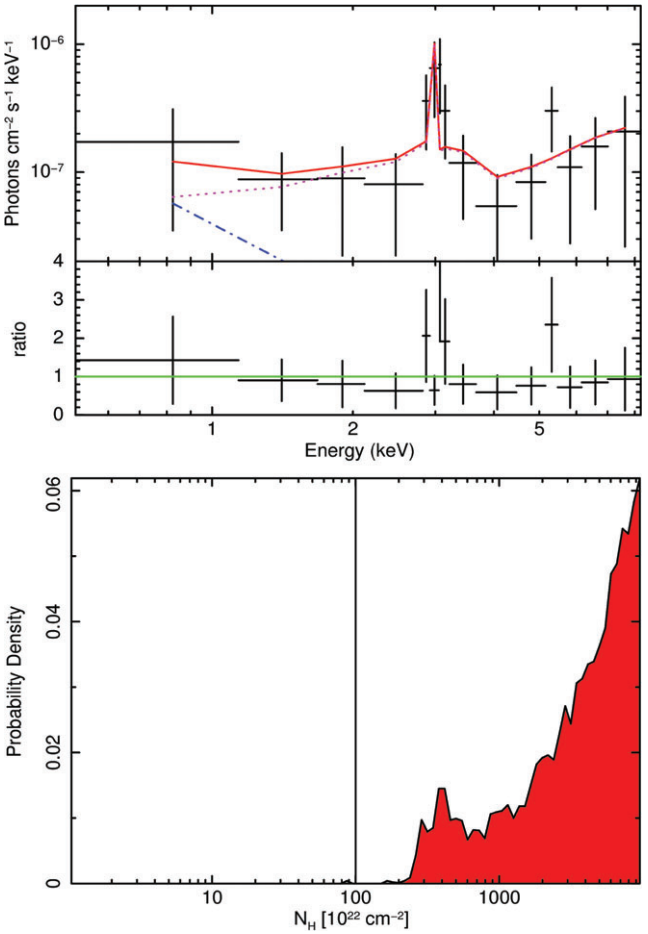

FIGURE 6 Same as Figure 5, for source LID_390.

lon et al. 2011) to $z > 1$ (40% based on only eight sources), while other authors have found no evolution of the CT fraction at high z (e.g., Buchner et al. 2015). We confirm the increase in the fraction of CT, especially at $2 < z < 3.5$, with a sample of 24 sources (the sum of all the probability distributions gives ~ 13 sources). This result is in agreement with the idea that at high redshift other factors such as the concentration of dense gas and dust clouds in the central region of the host galaxy (possibly induced by gas-rich mergers) may contribute to CT obscuration, on top of the canonical molecular torus (e.g., Hopkins et al. 2006).

3.2 | Extremely obscured CT

Of particular interest is the observed distribution of N_H above 10^{25} cm^{-2}, first of all because it is mostly unknown, even at low redshift (see e.g., Maiolino et al. 2003), and second because it is not possible to derive any estimate on the number of heavily CT sources with the indirect method of the CXB synthesis models.

Very few (e.g., Piconcelli et al. 2011; Gandhi et al. 2013, or the debated case of Arp220, Wilson et al. 2014) of these reflection-dominated sources is known in the local universe (see the compilation of Gandhi et al. 2014), and even more uncertain is their fraction above $z \sim 0.1$.

In Lanzuisi et al. (2015b), we have found the first $N_H = 10^{25}$ cm^{-2} CT AGN candidate in COSMOS, thanks to several multiwavelength indicators ([NeV], IR, and bolometric luminosity from SED). With the analysis presented here, we were able to find, only through X-ray spectral analysis, nine sources that have the N_H PDF completely above 10^{24} cm^{-2} and the upper boundary pegged at the upper limit of the model adopted $N_H(\text{up}) = 10^{26}$ cm^{-2} 2. Figures 5 and 6 show the spectra and PDF of two such reflection-dominated sources, where a very strong Fe Kα line is superimposed on a flat continuum. Most (7/9) of these sources have $z >$ ~ 1.5, because above these values both the Fe line and the Compton hump are easier to detect.

4 | CONCLUSIONS

Thanks to a combination of new, dedicated models and sophisticated analysis techniques, specifically developed for low-count statistics, recent works have found a growing number of CT AGN at high redshift in deep X-ray surveys (e.g., Brightman et al. 2014; Buchner et al. 2015). We applied a similar approach to the large catalog of X-ray detected AGN in the

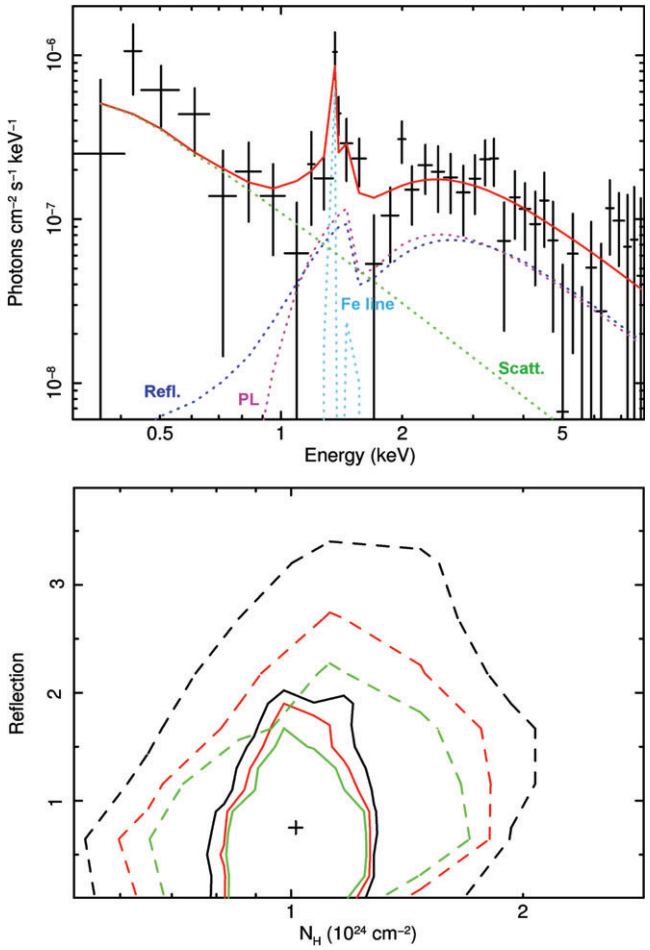

FIGURE 7 (a) Unfolded spectrum of source XID202 from the XMM-CDFS catalog, a CT AGN at $z = 3.7$. The different components (primary power law, reflection, Fe line complex, scattered emission) are labeled with different colors. (b) 99, 90, and 68% confidence contours obtained from the XMM–Newton spectrum (thick lines) and from the Chandra one (dotted lines) for N_H and the reflection fraction.

COSMOS-Legacy survey and demonstrated that not only are mildly CT sources up to $z \sim 3.5$ recoverable via X-ray spectral analysis but also reflection-dominated, heavily CT sources at $z \sim 2$ can be efficiently identified.

We underline, however, that X-rays need to be complemented by rich multiwavelength data, in order to verify that the solution at high N_H—and therefore high L_X—found for each of these sources is not only statistically motivated, given the available X-ray spectra, but also physically reasonable, given all the other multiwavelength data available.

4.1 | Implications for XMM-Newton

While Chandra is more efficient in detecting faint (high-z and/or obscured) sources[4], the spectra obtained with long XMM–Newton exposures have a much higher number of net counts (if the source is bright enough, i.e., a few$\times 10^{-15}$ erg cm^{-2} s^{-1}), and they allow us to constrain simultaneously the column density (even above 10^{25}) cm^{-2} and the reflection fraction, which are two crucial parameters for CXB models.

As an example, we show here the XMM–Newton spectrum of source XID-202 in the XMM-CDFS catalog (Ranalli et al. 2013). The nominal 3.4 Ms exposure time invested by XMM–Newton (corresponding to an effective exposure time of ~ 6 Ms between pn and MOS1+2) allowed the collection of $\sim 1{,}500$ total net counts (in Figure 7 we show only the pn spectrum for clarity) for this $z = 3.7$ CT source (Comastri et al. 2011). The spectral quality is high enough to allow us to use a more complex CT model (MYTorus, in the decoupled version) and constrain simultaneously the N_H and the reflection fraction (Figure 7 bottom panel, thick lines). On the other hand, the nominal 4 Ms collected with Chandra (3.6 effective exposure at the source position) give only 380 net counts. Despite the much lower background, the uncertainties on these parameters obtained from the Chandra spectrum are much larger (dashed lines).

Of course, sources of similar intrinsic luminosity ($L_X > 5 \times 10^{44}$ erg s^{-1}) at high redshift are rare (e.g., Vito et al. 2014). Therefore, the most efficient way to collect a decent sample (e.g., 10 sources) of high-redshift CT AGN at these flux levels ($F_{2-10} \sim 5 \times 10^{-15}$ erg cm^{-2} s^{-1}) for which all the different parameters of a complex CT model can be determined may be to spend long (e.g., 1 Ms) exposure times over CT candidates at high z selected in existing/ongoing large-area surveys, such as XMM-XXL (Pierre et al. 2016) or S82 (La Massa et al. 2013).

[4]By about a factor ~ 2, as can be derived comparing the total exposure time needed, and the number of CT AGN selected, in the Chandra (this work) and XMM–Newton (Lanzuisi et al. 2015a) catalogs of a medium/deep survey like COSMOS.

REFERENCES

Akylas, A., Georgakakis, A., Georgantopoulos, I., et al. (2012). *A&A*, *546*, A98.
Alexander, D. M., Stern, D., Del Moro, A., et al. (2013). *ApJ*, *773*, 125.
Ballantyne, D. R., Draper, A. R., Madsen, K. K., et al. (2011). *ApJ*, *736*, 56.
Brightman, M., & Nandra, K. (2011). *MNRAS*, *413*, 1206.
Brightman, M., Nandra, K., Salvato, M., et al. (2014). arXiv : 1406.4502
Brightman, M., & Ueda, Y. (2012). *MNRAS*, *423*, 702.
Buchner, J., Georgakakis, A., Nandra, K., et al. (2015). *ApJ*, *802*, 89.
Burlon, D., Ajello, M., Greiner, J., et al. (2011). *ApJ*, *728*, 58.
Cappelluti, N., Brusa, M., Hasinger, G., et al. (2009). *A&A*, *497*, 635.
Castello-Mor, N., Carrera, F. J., Alonso-Herrero, A., et al. (2013). *A&A*, *556*, A114.
Civano, F., Elvis, M., Brusa, M., et al. (2012). *ApJS*, *201*, 30.
Civano, F., Hickox, R. C., Puccetti, S., et al. (2015). *ApJ*, *808*, 185.
Civano, F., Marchesi, S., Comastri, A., et al. (2016). *ApJ*, *819*, 62.
Comastri, A., Gilli, R., Marconi, A., et al. (2015). *A&A*, *574*, L10.
Comastri, A., Ranalli, P., Iwasawa, K., et al. (2011). *A&A*, *526*, L9.
Comastri, A., Setti, G., Zamorani, G., & Hasinger, G. (1995). *A&A*, *296*, 1.
Delvecchio, I., Lutz, D., Berta, S., et al. (2015). *MNRAS*, *449*, 373.
Elvis, M., Civano, F., Vignali, C., et al. (2009). *ApJS*, *184*, 158.
Fiore, F., Grazian, A., Santini, P., et al. (2008). *ApJ*, *672*, 94–101.
Gandhi, P., Horst, H., Smette, A., et al. (2009). *A&A*, *502*, 457.
Gandhi, P., Terashima, Y., Yamada, S., et al. (2013). *ApJ*, *773*, 51.
Gandhi, P., Annuar, A., Alexander, D. M., et al. (2014), Suzaku-MAXI 2014: Expanding the Frontiers of the X-ray Universe, 319.
Georgantopoulos, I., Comastri, A., Vignali, C., et al. (2013). *A&A*, *555*, A43.
Georgantopoulos, I., Dasyra, K. M., Rovilos, E., et al. (2011). *A&A*, *531*, A116.
Gilli, R., Comastri, A., & Hasinger, G. (2007). *A&A*, *463*, 79.
Gilli, R., Vignali, C., Mignoli, M., et al. (2010). *A&A*, *519*, AA92.

Hasinger, G., Cappelluti, N., Brunner, H., et al. (2007). *ApJS*, *172*, 29.
Hopkins, P. F., Somerville, R. S., Hernquist, L., et al. (2006). *ApJ*, *652*, 864.
Houck, J. R., Soifer, B. T., Weedman, D., et al. (2005). *ApJ*, *622*, L105.
Ilbert, O., Capak, P., Salvato, M., et al. (2009). *ApJ*, *690*, 1236.
Kormendy, J., & Ho, L. C. (2013). *ARA&A*, *51*, 511.
La Massa, S. M., Urry, C. M., Cappelluti, N., et al. (2013). *MNRAS*, *436*, 3581.
Lacy, M., Storrie-Lombardi, L. J., Sajina, A., et al. (2004). *ApJS*, *154*, 166.
Lanzuisi, G., Civano, F., Elvis, M., et al. (2013). *MNRAS*, *431*, 978.
Lanzuisi, G., Perna, M., Delvecchio, I., et al. (2015a). *A&A*, *578*, A120.
Lanzuisi, G., Piconcelli, E., Fiore, F., et al. (2009). *A&A*, *498*, 67.
Lanzuisi, G., Ranalli, P., Georgantopoulos, I., et al. (2015b). *A&A*, *573*, AA137 (L15).
Maiolino, R., Comastri, A., Gilli, R., et al. (2003). *MNRAS*, *344*, L59.
Marchesi, S., Civano, F., Elvis, M., et al. (2016a). *ApJ*, *817*, 34.
Marchesi, S., Lanzuisi, G., Civano, F., et al. (2016b). arXiv:1608.05149
Marconi, A., Risaliti, G., Gilli, R., et al. (2004). *MNRAS*, *351*, 169.
Martinez-Sansigre, A., Rawlings, S., Lacy, M., et al. (2005). *Nature*, *436*, 666.
Mignoli, M., Vignali, C., Gilli, R., et al. (2013). *A&A*, *556*, A29.
Murphy, K. D., & Yagoob, T. (2009). *MNRAS*, *397*, 1549.
Piconcelli, et al. (2011).
Pierre, M., Pacaud, F., Adami, C., et al. (2016). *AAP*, *592*, A1.
Ranalli, P., Comastri, A., Vignali, C., et al. (2013). *A&A*, *555*, A42.
Risaliti, G., Maiolino, R., & Salvati, M. (1999). *ApJ*, *522*, 157.
Salvato, M., Ilbert, O., Hasinger, G., et al. (2011). *ApJ*, *742*, 61.
Scoville, N., Aussel, H., Brusa, M., et al. (2007). *ApJS*, *172*, 1.
Soltan, A. (1982). *MNRAS*, *200*, 115.
Stern, D. (2015). *ApJ*, *807*, 129.
Suh, et al. (2016).
Suh et al. 2017 submitted
Tozzi, P., Gilli, R., Mainieri, V., et al. (2006). *A&A*, *451*, 457.
Treister, E., Urry, C. M., & Virani, S. (2009). *ApJ*, *696*, 110.
Ueda, Y., Akiyama, M., Hasinger, G., et al. (2014). *ApJ*, *786*, 104.
Vignali, C., Alexander, D. M., & Comastri, A. (2006). *MNRAS*, *373*, 321.
Vignali, C., Mignoli, M., Gilli, R., et al. (2014). *AAP*, *571*, A34.
Vito, F., Gilli, R., Vignali, C., et al. (2014). *MNRAS*, *445*, 3557.
Zappacosta, et al. (2017), Submitted.

How to cite this article: Lanzuisi G. X-ray selection of Compton-Thick AGN at high redshift, *Astron. Nachr./AN*. 2017;338:316–322. https://doi.org/10.1002/asna.201713349.